Title

Microglial repopulation model reveals a robust homeostatic process for replacing CNS myeloid cells

Journal

Proceedings of the National Academy of Sciences of the United States of America, 109(44)

ISSN

0027-8424

Authors

Varvel, Nicholas H
Grathwohl, Stefan A
Baumann, Frank
et al.

Publication Date

2012-10-30

DOI

10.1073/pnas.1210150109

Peer reviewed

Microglial repopulation model reveals a robust homeostatic process for replacing CNS myeloid cells

Nicholas H. Varvel[a,b,1,2], Stefan A. Grathwohl[a,b,1,2], Frank Baumann[a,b], Christian Liebig[a,b], Andrea Bosch[a,b], Bianca Brawek[c], Dietmar R. Thal[d], Israel F. Charo[e], Frank L. Heppner[f], Adriano Aguzzi[g], Olga Garaschuk[c], Richard M. Ransohoff[h], and Mathias Jucker[a,b,2]

[a]German Center for Neurodegenerative Diseases (DZNE) and [b]Department of Cellular Neurology, Hertie Institute for Clinical Brain Research, University of Tuebingen, 72076 Tuebingen, Germany; [c]Institute of Physiology II, University of Tuebingen, 72074 Tuebingen, Germany; [d]Laboratory of Neuropathology, Institute of Pathology, University of Ulm, 89081 Ulm, Germany; [e]Gladstone Institute of Cardiovascular Disease, University of California, San Francisco, CA 94158; [f]Department of Neuropathology, Charité–Universitätsmedizin Berlin, 10117 Berlin, Germany; [g]Institute of Neuropathology, Department of Pathology, University Hospital Zurich, 8091 Zurich, Switzerland; and [h]Neuroinflammation Research Center, Department of Neurosciences, Lerner Research Institute, Cleveland Clinic, Cleveland, OH 44195

Edited by Don W. Cleveland, University of California at San Diego, La Jolla, CA, and approved September 19, 2012 (received for review June 14, 2012)

Under most physiological circumstances, monocytes are excluded from parenchymal CNS tissues. When widespread monocyte entry occurs, their numbers decrease shortly after engraftment in the presence of microglia. However, some disease processes lead to focal and selective loss, or dysfunction, of microglia, and microglial senescence typifies the aged brain. In this regard, the long-term engraftment of monocytes in the microglia-depleted brain remains unknown. Here, we report a model in which a niche for myeloid cells was created through microglia depletion. We show that microglia-depleted brain regions of *CD11b-HSVTK* transgenic mice are repopulated with new Iba-1-positive cells within 2 wk. The engrafted cells expressed high levels of CD45 and CCR2 and appeared in a wave-like pattern frequently associated with blood vessels, suggesting the engrafted cells were peripheral monocytes. Although two times more numerous and morphologically distinct from resident microglia up to 27 wk after initial engraftment, the overall distribution of the engrafted cells was remarkably similar to that of microglia. Two-photon in vivo imaging revealed that the engrafted myeloid cells extended their processes toward an ATP source and displayed intracellular calcium transients. Moreover, the engrafted cells migrated toward areas of kainic acid-induced neuronal death. These data provide evidence that circulating monocytes have the potential to occupy the adult CNS myeloid niche normally inhabited by microglia and identify a strong homeostatic drive to maintain the myeloid component in the mature brain.

chemokines | myeloid cell heterogeneity | neuroinflammation | in vivo calcium imaging

Microglia, the brain-resident myeloid cells, populate brain tissue early in development (1, 2). Microglia continuously monitor some synapses (3, 4), palpate cerebral blood vessels, astrocytes, and interact with neighboring microglia (5, 6) and play a role in synaptic pruning (7). Injuries to the central nervous system (CNS) induce microgliosis, a condition characterized by microglia proliferation, morphological transformation, and increased expression of cytokines and chemokines (8–10). Microgliosis can have beneficial as well as detrimental consequences, likely mediated by the nature of the initial insult as well as duration of the inflammatory response (11).

Monocytes do not enter the healthy CNS parenchyma (12, 13). Under defined experimental conditions, however, circulating monocytes can infiltrate CNS tissue and contribute to the neuroimmune response (13, 14). Interestingly, monocytes, like microglia, can also exacerbate or mitigate disease phenotypes. For example, depleting perivascular monocytes (15) or inhibiting their entry into the CNS (16, 17) worsens β-amyloid pathology in Alzheimer's disease mouse models. In contrast, depletion of monocytes (18) or blocking infiltration (19, 20) into the CNS in experimental autoimmune encephalitis (EAE) markedly reduces disease severity.

Our understanding of monocyte entry, engraftment, and persistence in CNS tissues has been obtained in the context of a full complement of resident microglia. However, resident microglia are lost or can become dysfunctional in certain CNS disorders and during aging (21–25). Thus, the competence of circulating monocytes to respond to microglial loss or complete dysfunction is unknown. In the present study, we show that upon microglia depletion engrafted myeloid cells take up long-term CNS residence and assume some functional properties of microglia.

Results

Repopulation of Microglia-Depleted Mice. We replicated previous findings (26) that intracerebroventricular ganciclovir (GCV) (50 mg/mL) treatment for 2 wk leads to almost complete ablation of microglia (>90%) in the neocortex of *CD11b-HSVTK* (TK+) mice with the remaining microglia exhibiting superramified morphology with numerous branched processes (Fig. 1*A*). In contrast, GCV treatment did not alter the number or morphology of the resident microglia in TK− control mice (Fig. 1*B*). The microglia ablation was confirmed in methylene blue-stained semithin sections (Fig. S1).

To determine whether the microglia-free neocortical areas became repopulated with new myeloid cells after GCV treatment discontinuation, TK+ mice were again treated with GCV for 2 wk with subsequent removal of the osmotic pump reservoir. Histological examination of the brain tissue was performed 2 wk after GCV termination. Strikingly, and in contrast to brain tissue from TK+ mice killed immediately after the 2-wk GCV application, ionized calcium binding adapter molecule 1 (Iba1)-positive cells were encountered throughout the neocortex of TK+ animals, suggesting that these cells populated the brain during the 2 wk after GCV treatment was suspended (Fig. 1*A*). Notably, in the TK+ mice, the newly engrafted Iba1-positive cells oriented themselves in a pattern similar to resident microglia in TK− controls, but also appeared more numerous and demonstrated distinct morphological alterations consisting of shorter, asymmetrically oriented processes as well as enlarged cell bodies throughout the neocortex (Fig. 1*A*). Additional mice were

Author contributions: N.H.V., S.A.G., C.L., D.R.T., R.M.R., and M.J. designed research; N.H.V., S.A.G., C.L., A.B., B.B., D.R.T., and O.G. performed research; I.F.C. and F.L.H. contributed new reagents/analytic tools; N.H.V., S.A.G., F.B., C.L., B.B., D.R.T., F.L.H., A.A., O.G., R.M.R., and M.J. analyzed data; and N.H.V., S.A.G., C.L., R.M.R., and M.J. wrote the paper.

The authors declare no conflict of interest.

This article is a PNAS Direct Submission.

[1]N.H.V. and S.A.G. contributed equally to this work.

[2]To whom correspondence may be addressed. E-mail: nicholas.varvel@dzne.de, S.Grathwohl@gmx.de, or mathias.jucker@uni-tuebingen.de.

This article contains supporting information online at www.pnas.org/lookup/suppl/doi:10.1073/pnas.1210150109/-/DCSupplemental.

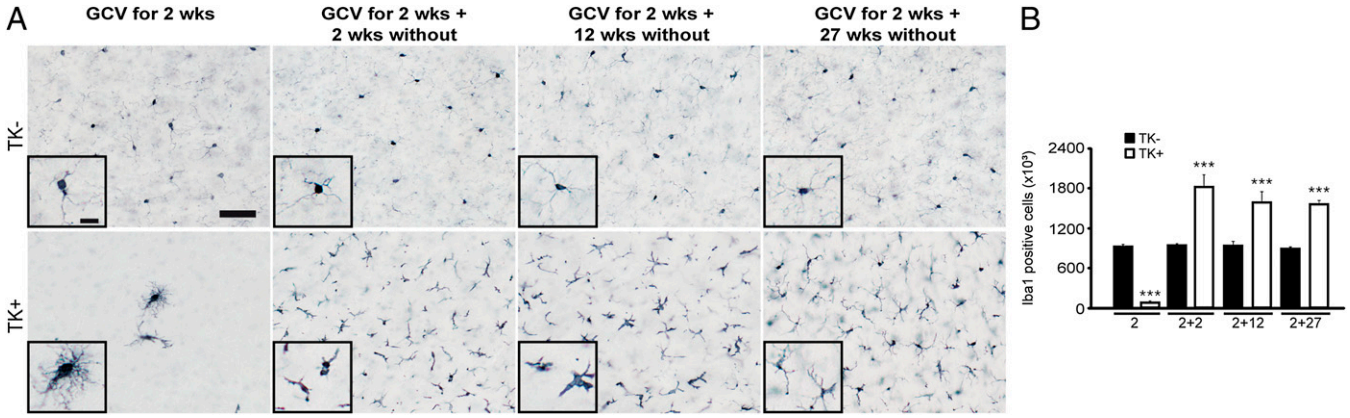

Fig. 1. After microglia depletion, Iba1-positive cells repopulate the brain. (*A*) Iba1 immunohistology revealed nearly complete microglia depletion in the neocortex of TK+ mice after 2 wk of treatment. Note that the remaining cells are highly ramified microglia (*Inset*), whereas microglia in TK− mice were not affected by the treatment. In TK+ mice, termination of GCV treatment led to robust infiltration of new Iba1+ cells in the neocortex over the following 2 wk, and the distinct morphology was maintained both 12 and 27 wk after initial infiltration. (Scale bar, 50 μm.) (*B*) Stereological analysis of total Iba1+ cells in the neocortex revealed a >90% ablation of microglia in TK+ mice after 2 wk of GCV treatment (indicated is the mean ± SEM; $n = 7$ mice/genotype; all mice were male). Note that before GCV application TK+ and TK− mice do not differ in microglia number (26). Two, 12, and 27 wk after GCV treatment discontinuation, the number of Iba1+ cells in TK+ mice exceeded the amount of microglia in TK− control littermates by approximately twofold ($n = 6$ mice/genotype for 2 + 2 wk; $n = 7$ and 5 mice/genotype for 2 + 12 wk and 3 mice/genotype for 2 + 27 wk; all mice were male). ANOVA revealed a significant interaction of Transgene by Time points [$F_{(7,43)} = 35.27$; $^{***}P < 0.001$]. Tukey HSD post hoc analysis revealed significant differences between the TK− and TK+ mice at all time points.

analyzed 12 and 27 wk after GCV termination. After these prolonged incubation periods, the Iba1-positive cells revealed a distribution pattern similar to resident microglia but continued to display an altered morphology distinguishable from resident microglia (Fig. 1*A*). Quantitative stereological analysis indicated that ~1.8×10^6 Iba1-positive cells engrafted in the neocortex during the 2 wk following termination of GCV treatment. This value was approximately double the number of resident microglia encountered in control animals (Fig. 1*B*), confirming the histological observations. The number of Iba1-immunoreactive cells remained stable over all time points analyzed (Fig. 1*B*).

To determine whether the new myeloid cells first appeared in one neocortical brain region or whether they originated from multiple locations, microglia were again depleted for 2 wk. Histological analysis was performed 1 wk after terminating GCV treatment. Results revealed densely populated areas of Iba1-positive cells at multiple locations along the rostral-caudal axis in microglia-depleted TK+ mice (Fig. S2). Notably, the infiltrating cells appeared to enter the brain from capillary or small blood vessels (Fig. S2). These "waves of infiltrating myeloid cells" were common in the brain areas where microglia depletion was robust. In extreme rostral and caudal regions of the neocortex and in the cerebellum, where remaining resident microglia were more numerous, the engrafted myeloid cells were less common, consistent with a homeostatic replacement of the CNS myeloid component (Fig. S3).

Nature and Origin of the Newly Engrafted Myeloid Cells. The engrafted cells expressed higher levels of CD45 compared with resident microglia in the TK− controls (Fig. 2*A*), suggesting a peripheral origin. Antibodies toward CD68 and CD11b revealed no qualitative differences between TK− and TK+ mice, and the newly appearing cells were not immunoreactive for CD11c or CD206 (Fig. 2*B*). Proliferation of the newly appearing Iba1-positive cells in the TK+ mice was similar to that of resident microglia in the TK− mice (Fig. 2*C*).

To support the possibility that the newly engrafted myeloid cells originate from the periphery, microglia were depleted for 2 wk in green fluorescent protein (*gfp*) bone marrow TK chimeras and killed 2 wk later (Fig. 3*A*). Although resident microglia were not depleted in chimeric TK− animals and only a few GFP-positive cells were observed in the brain parenchyma, GFP-positive cells were visible throughout the neocortex of microglia depleted TK+ mice (Fig. 3*A*). The bone marrow-derived GFP-positive cells displayed short, asymmetrically oriented processes as well as enlarged cell bodies.

To assess the peripheral origin of engrafted cells with an irradiation-independent system, microglia were depleted in TK+/*Ccr2*$^{+/rfp}$ mice for 2 wk and the animals were killed 1 wk after terminating GCV treatment. Consistent with previous reports (27), CCR2-RFP expression was not observed in TK−/*Ccr2*$^{+/rfp}$ control mice. In contrast, clusters of CCR2-RFP–positive cells were encountered in close proximity to cerebral blood vessels in TK+/*Ccr2*$^{+/rfp}$ mice (Fig. 3*B*). Some CCR2-RFP–expressing cells were not Iba1-positive and were likely infiltrating monocytes that have not differentiated into macrophages (12). Because CCR2-expressing cells infiltrated into microglia-depleted brain, whole-brain homogenates were analyzed for expression of CCL2, the major CNS ligand for CCR2. Brain levels of CCL2 were increased sevenfold in microglia-depleted TK+ mice compared with TK− controls. However, CCL2 levels were no longer increased after the engraftment of myeloid cells (Fig. S4). Differences in blood serum levels of CCL2 and alterations in inflammatory cytokines TNF-α and IL-6 were not encountered (Fig. S4).

Newly Engrafted Myeloid Cells Function in Similar Fashion as Microglia. Microhemorrhages and myelotoxicity have been observed in TK+ mice treated with GCV for 4 wk (26). Therefore, the current experiments were designed to avoid these adverse effects by reducing the duration of GCV treatment. Notably, no microhemorrhages could be detected with this protocol. No obvious disruption of neocortical architecture and no alterations in neuronal number were apparent in TK+ mice compared with controls at the 12-wk time point (Fig. S5). However, as previously reported for the microglia-depleted brain areas (26), astrocytosis was detectable at all time points examined. As a broad indication of animal well-being, no differences in body weight were found in TK+ compared with TK− mice (Fig. S5). Significant alterations in numbers of leukocytes, erythrocytes, or thrombocytes were also not encountered (Fig. S5). The percentages of lymphocytes, monocytes, and granulocytes were also unaltered within the leukocyte pool of cells (Fig. S5). These

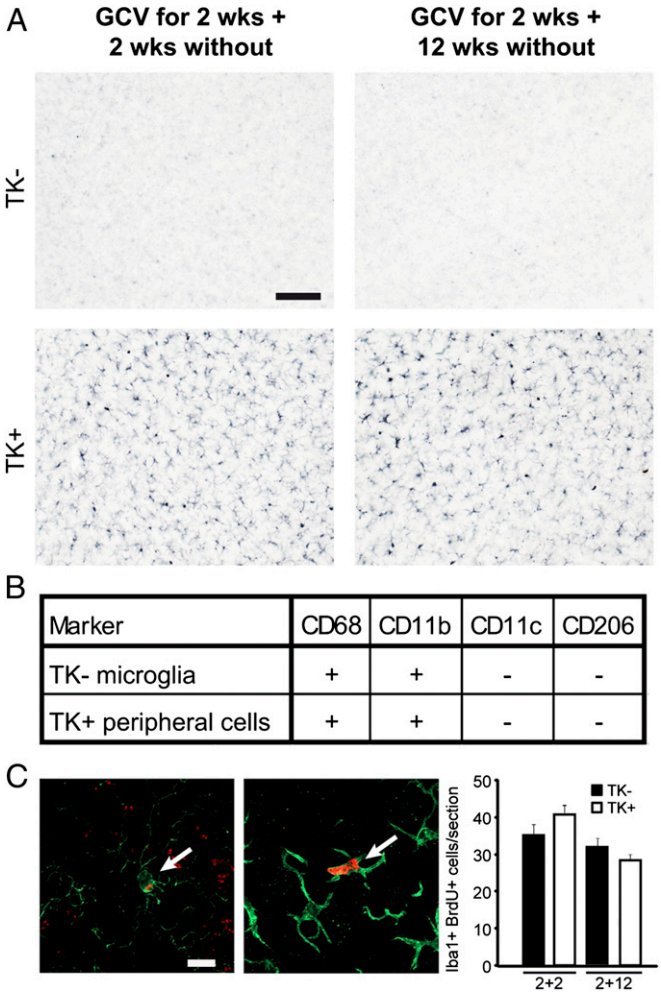

Fig. 2. Infiltrating cells are CD45^{high} in microglia-depleted TK+ mice and show similar proliferation as microglia. (*A*) Microglia in TK− mice expressed low levels of CD45, characteristic of resident microglia. In contrast, the newly appearing cells had markedly higher CD45 levels at 2 + 2 and 2 + 12 wk. (Scale bar, 100 μm.) (*B*) Other markers did not differ between microglia and infiltrating cells TK− and TK+ mice, respectively (+, positive staining; −, no staining). (*C*) Double, fluorescent immunohistochemistry for Iba1 (green) and BrdU (red) revealed the presence of double-labeled BrdU+/Iba1+ cells (arrow) in TK− (*Left*) and repopulated TK+ (*Center*) mice. (Scale bar, 10 μm.) The numbers of BrdU+ myeloid cells was similar in both conditions and time points examined.

results show that, besides astrocytosis, no grossly evident deleterious side effects are encountered after microglia ablation and myeloid cell repopulation.

Computer-assisted image analysis and 3D surface reconstruction of Iba1-labeled microglia and newly populated myeloid cells were performed to determine whether the newly engrafted cells covered the neuropil in similar fashion as resident microglia (Fig. 4). Results revealed that most areas of the neuropil were <6 μm from the nearest microglia in the TK− mice, and compatible observations were made for the infiltrating myeloid cells in the TK+ mice. Few areas of the neuropil were identified at distances >6 μm from the nearest microglia or from newly engrafted cells (Fig. 4). These findings highlight the shared ability of both microglia and newly populated myeloid cells to position their cell bodies and extend their processes into the surrounding neuropil.

To study the in vivo function of the newly engrafted myeloid cells in comparison with resident microglia, an isolectin B4-based labeling technique was used (28). Results revealed that the newly engrafted cells had shorter and asymmetrically oriented processes (Fig. 5*A*, *Left*). Upon the insertion of an ATP-containing pipette, the myeloid cell's processes extended toward the tip of the pipette (Fig. 5*A*, *Center*). Next, the newly populated myeloid cells were labeled with a calcium-sensitive indicator dye, Oregon Green BAPTA 1 (OGB-1) (via electroporation). Intracellular Ca^{2+} transients were observed in all of the newly engrafted cells in response to ATP and UDP and 75% responded to a local 2′(3′)-*O*-(4-benzoylbenzoyl)-ATP (Bz-ATP) application (Fig. 5*B*). The decay kinetics of the ATP-, Bz-ATP–, and UDP-evoked calcium transients in the engrafted monocytes was not significantly different than those encountered in resident microglia (Fig. S6). Also, no differences in the peak amplitude of ATP-induced calcium transients were observed. However, at the stage of the engraftment tested, the amplitudes of UDP- and Bz-ATP–evoked calcium transients were significantly larger in monocytes compared with microglia (Fig. S6). Thus, the engrafted cells respond to extracellular signaling molecules in a microglia-like fashion by process extension and initiating intracellular calcium transients. The amplitude and kinetics of these transients are largely similar, but not identical with those encountered in microglia.

To determine whether the engrafted myeloid cells are also responsive to CNS injury, repopulated TK+ mice were exposed to kainic acid (KA) to induce seizures and neuronal cell death in the hippocampus (29, 30). Substantial CA1 neurodegeneration was evident in the repopulated TK+ mice subjected to KA and the engrafted myeloid cells were now tightly clustered around the damaged CA1 region (Fig. S7). These findings provide evidence that the newly engrafted myeloid cells were capable of actively surveying their microenvironment and reacting to acute neuronal damage.

Discussion

In the present study, we established and characterized a microglia repopulation model. Our findings suggest that blood-derived monocytes infiltrate and engraft in the microglia-depleted mouse brain regions. Myeloid cell engraftment was robust and rapid, as ~1.8×10^6 Iba1-positive cells repopulated the brain within 2 wk. The cellular engraftment observed in the current study is reminiscent of previous studies performed on *PU.1*$^{-/-}$ mice (24). However, in *PU.1*$^{-/-}$ mice, myeloid cells repopulated the CNS only after wild-type bone marrow reconstitution because *PU.1*$^{-/-}$ mice are not only devoid of microglia but also circulating monocytes and tissue macrophages (24).

Although short-term elimination of microglia in mice under controlled and specific pathogen-free conditions appears not to be deleterious (26), the long-term consequences of microglia removal have been difficult to evaluate. *PU.1*$^{-/-}$ mice die early in life without bone marrow reconstitution (24, 31), and TK+ mice experience myelotoxicity when treated with GCV for prolonged time (26, 32). In both models, peripheral, hematopoietic side effects are likely the main contributing factors of the lethal phenotype. Nevertheless, long-term elimination or dysfunction of microglia likely has deleterious consequences on CNS homeostasis as exemplified in neurodegenerative conditions, such as Nasu–Hakola disease or Rett syndrome (22, 33, 34).

In both the bone marrow-reconstituted *PU.1*$^{-/-}$ animals (24) and the repopulated TK+ mice, obvious deleterious phenotypes are not evident. There was no change in body weight in GCV-treated TK+ mice compared with TK− controls during the entire observation period of 27 wk. Cortical architecture and neuronal numbers were unaltered in the engrafted TK+ animals, and no indication of neurodegeneration was found. Taken together, these findings suggest that the newly engrafted myeloid cells are recruited to take over housekeeping roles to maintain CNS homeostasis in similar fashion as microglia. This is consistent with the observation that myeloid cells engrafted only in the microglia-depleted brain regions.

Our data suggest that engrafting cells are of peripheral origin and mainly enter the brain from small blood vessels or

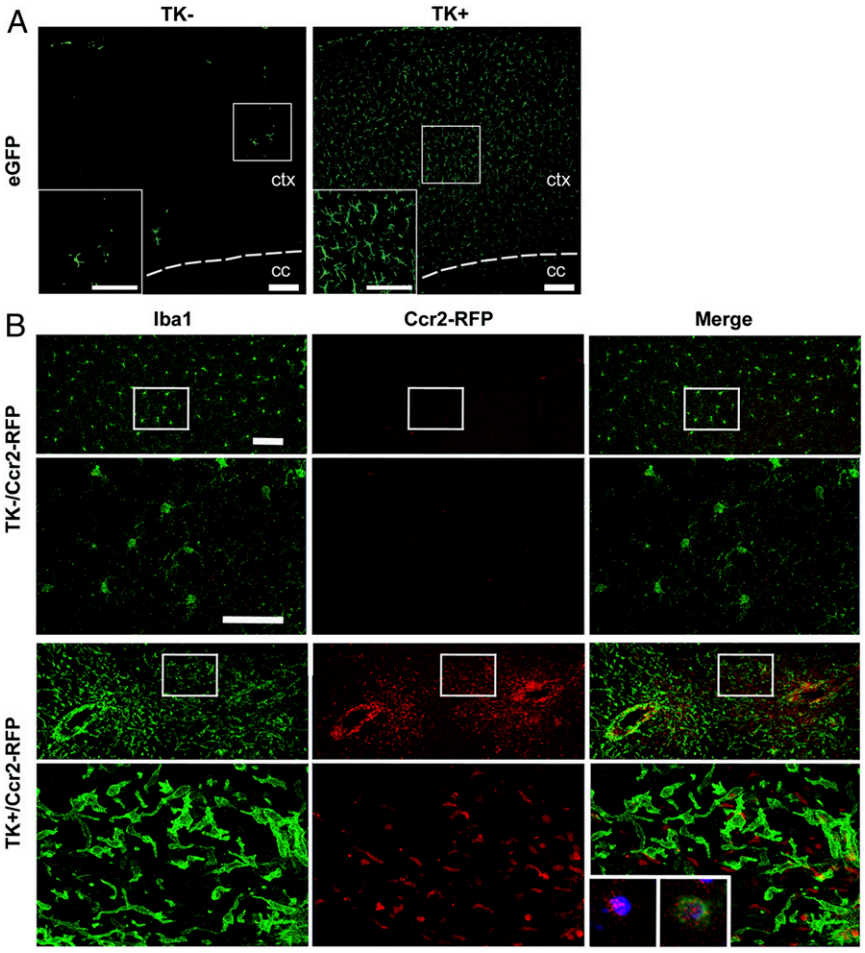

Fig. 3. Infiltrating cells are of peripheral origin. (*A*) Few bone marrow-derived eGFP-positive cells are observed in the neocortex (*Inset*) of reconstituted TK− animals [shown are the neocortex (ctx) and corpus callosum (cc)]. eGFP-positive cells with similar morphology to infiltrating monocytes (i.e., large cell body with short and ramified processes) were observed in the microglia-ablated TK+ mice ($n = 3$ mice/genotype). *Insets* are a higher magnification of the boxed areas. (Scale bars, 100 μm.) (*B*) Maximum projection fluorescent images of Iba1 immunohistochemistry (green) revealed resident microglia uniformly positioned in the cortex in TK−/*Ccr2*$^{+/rfp}$ animals. CCR2-expressing cells are absent from the cortical parenchyma (red). (Scale bar, 100 μm.) Bottom panels for each genotype are higher magnification images. (Scale bar, 50 μm.) Microglia-depleted TK+/*Ccr2*$^{+/rfp}$ mice revealed patches of infiltrating Iba1-immunoreactive (green) and CCR2-expressing cells (red) in the cortex. Higher magnification images showed that Iba1 and CCR2-RFP signals occurred within the same area. However, 100% overlap of the two signals was not observed. A single projection image (*Left Inset* in merge) shows only CCR2-RFP signal (red). Other cells were encountered (*Right Inset* in merge) with both CCR2-RFP (red) and Iba1 (green) signals within one cell. In the *Insets*, the cell nuclei are stained with DAPI (blue).

capillaries. Nevertheless, the possibility that GCV treatment compromises the blood–brain barrier (BBB), leading to a general engraftment of peripheral cells, cannot be excluded. Indeed, extravascular IgG deposition (but no hemosiderin staining) was observed in microglia-depleted/repopulated mouse brain, at the time points examined, suggesting compromise of the BBB. Recent evidence indicates that pericyte dysfunction can contribute to loss of BBB function (35, 36). However, no evidence of PDGF receptor-β–positive pericyte loss was encountered in our model. Moreover, brain CCL2 levels were elevated before the engraftment of the cells in TK+ mice and subsequently returned to baseline levels after monocyte engraftment.

The CNS invasion of CCR2-RFP–positive monocytes appeared limited to the period immediately following microglia depletion. Thus, it cannot completely be ruled out that the initial, engrafting population of monocytes dies off and is subsequently replaced by microglia cells generated from resident microglial progenitors and/or a CCR2-negative population of peripheral monocytes. However, the numbers of newly engrafted cells in the repopulated TK+ mice remained remarkably stable over the entire 27-wk observation period. In addition, the numbers of proliferating (BrdU-labeled) engrafted monocytes in TK+ mice were similar to the numbers of proliferating resident microglia in TK− mice at the time points examined. Thus, we speculate that the newly infiltrating monocytes are long-lived. This appears in contrast to a previous study reporting that infiltrates of peripheral monocytes persisted <3 mo in a mouse model of EAE (12). It is likely that the presence or absence of resident microglia determines the long-term engrafting potential of infiltrating myeloid cells.

Phenotypic characterization of the engrafting monocyte population revealed similarities and differences from resident microglia. As expected, neither cell type expressed mannose receptor, CD206, suggesting the infiltrates were not perivascular macrophages (15, 37). Our analysis identified CD11b and CD68 expression in both TK− (microglia) and TK+ (engrafted monocytes) mice. However, CD45 expression was higher in the engrafted population, in line with the idea that the new population was of peripheral origin. Indeed, CCR2 expression was encountered in the infiltrating monocytes. Expression of CD11c was not encountered in the engrafted monocytes, in contrast to other models of peripheral macrophage infiltration (38–40).

Morphologically, the newly engrafted myeloid cells were more numerous and had shorter processes than resident microglia. Although these morphological characteristics might be attributed to either the ontogeny of the newly engrafted cells or their reaction to the microglia-free environment, our findings revealed that the pattern of the engrafted cells and the coverage of the neuropil by their processes were nearly identical. These findings suggest that, in the adult brain, the newly engrafted myeloid cells could perform surveillance and scavenging functions similar to microglia.

Finally, in vivo imaging revealed that the newly engrafted cells were capable of process convergence toward extracellular ATP, similar to resident microglia (6). Moreover, we found that the capability of the newly engrafted monocytes to initiate Ca^{2+} transients was again similar to that observed in microglia, i.e., the transients were evoked by ATP as well as ionotropic and metabotropic P2 receptor agonists (28). Although the ATP-induced calcium transients in resident microglia and engrafted monocytes were similar in terms of their amplitude and decay

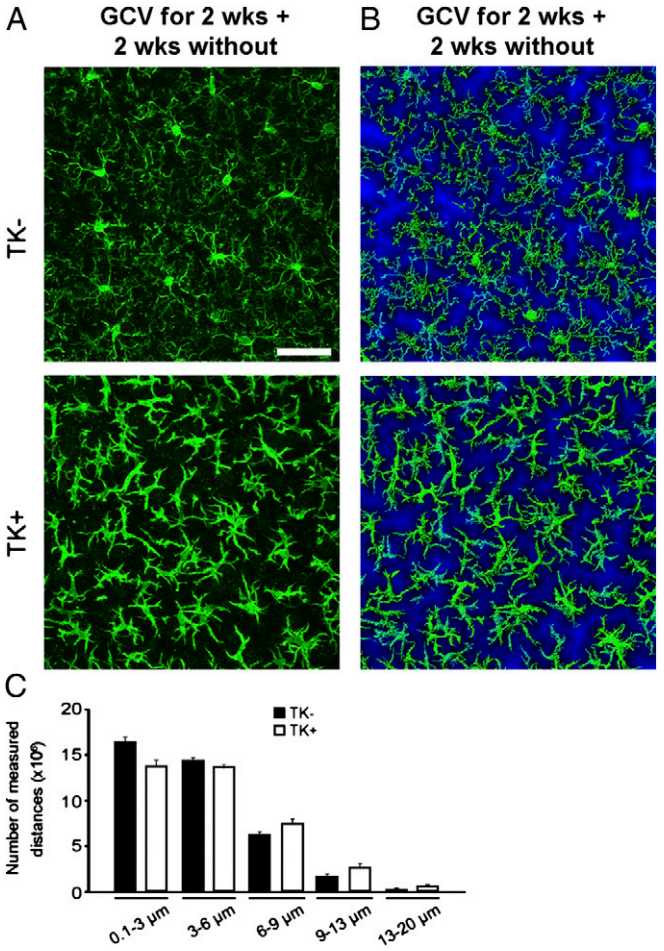

Fig. 4. Resident microglia and monocytes equally cover the neuropil with their processes. (*A*) Confocal imaging revealed Iba1-positive microglia in the TK− mice (*Upper*) and the infiltrating monocytes in the TK+ animals (*Lower*). (Scale bar, 40 μm.) (*B*) Three-dimensional surface area reconstruction of microglia in TK− mice (*Upper*) and infiltrating cells in TK+ animals (*Lower*) with a distance map (blue) to determine the distance from the nearest cellular process. A brighter blue signal represents greater distances. (*C*) Histogram of the distance maps shows no differences ($n = 5$ mice/genotype; all mice were male).

kinetics, we did encounter differences in the amplitudes of Bz-ATP– and UDP-evoked calcium transients.

These data show that, at least at the time point tested, the properties of newly engrafted monocytes are largely similar, but not (yet) identical with those of resident microglia.

The engrafted monocytes were capable of migrating to and sending processes toward acute KA-induced neuronal damage, also in similar fashion as microglia (41, 42). Nevertheless, it remains to be determined whether the mechanisms that promote cellular migration to damaged neural tissue are similar in the repopulated brain compared with the natural environment in this KA-induced lesion paradigm. The shared ability of both cell types to respond to ATP and other P2 receptor agonists suggests that the signaling pathways may be the same. Taken together, our findings suggest that engrafted myeloid cells are active monitors of the surrounding tissue.

A beneficial impact of monocytic engraftment in CNS tissue has been demonstrated in spinal cord injury (43) and retinal neuropathologies (44). Additionally, in AD mouse models, bone marrow-derived macrophages have been shown to limit plaque growth (45) and genetically modified monocytes can modulate AD pathology (46). Importantly, microglial apoptosis has been implicated in X-linked adrenoleukodystrophy (ALD) (21), and beneficial clinical outcomes have been reported in ALD patients subject to therapies using nonmutant myeloid cells (47). Furthermore, replacement of dysfunctional microglia through wild-type bone marrow transplantation resulted in improved functional outcome in a mouse model of Rett syndrome (22). These studies imply that it may be possible to exploit a homeostatic drive to maintain the CNS myeloid component in clinical situations. However, it has not previously been tested whether peripheral monocytes can indeed replace microglia that have become dysfunctional. Our data now suggest that, upon removal of microglia, peripheral myeloid cells repopulate microglia-depleted brain regions. Our work provides evidence that circulating monocytes have the potential to occupy the adult CNS myeloid niche inhabited by microglia and take over the essential surveillance functions normally performed by resident microglia.

Materials and Methods

Subjects and GCV Application. CD11b-HSVTK (TK) mice express a herpes simplex virus thymidine kinase (HSVTK) under the monocytic CD11b promoter (32). Male *Ccr2*$^{rfp/rfp}$ animals were mated to TK+ females. For the KA studies, female TK+ mice were bred to nontransgenic FVB males. Valganciclovir was delivered intacerebroventricularly as described (26). For details, see *SI Materials and Methods*.

Tissue Preparation, Histology, and Stereology. Paraformaldehyde-fixed free-floating serial sections were used. For details and antibodies, see *SI Materials and Methods*.

Analysis of Cytokine and Chemokine Levels. Cytokine protein levels of blood serum and whole-brain homogenates were measured using a multiplexed particle-based flow-cytometric cytokine assay. For details, see *SI Materials and Methods*.

In Vivo Two-Photon Imaging and Monocyte Labeling. Surgery was performed as described previously (48, 49). Engrafted cells were labeled with a calcium-sensitive indicator dye OGB-1 (Molecular Probes) by means of single-cell

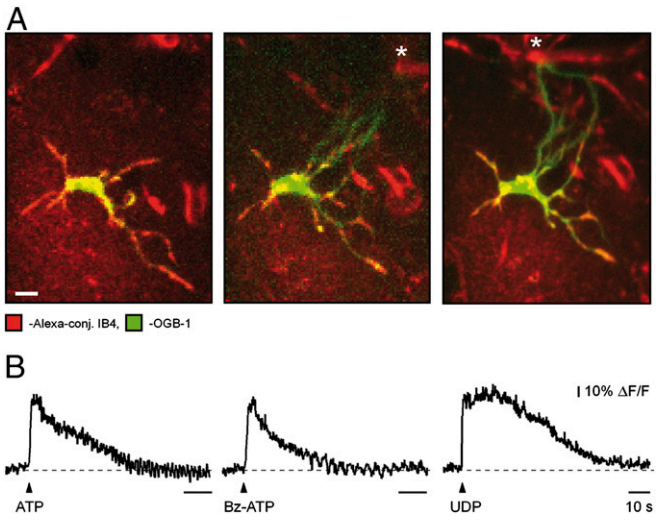

Fig. 5. Engrafted monocytes send processes toward an ATP-containing pipette and display Ca^{2+} transients in vivo. (*A*) Maximum-intensity projection image (55-78 μm depth; step, 1 μm) of a monocyte labeled with isolectin B4 conjugated to Alexa 594 (red) and OGB-1 (green) before (*Left*; 55–78 μm), 17 min (*Center*; 52–78 μm), and 76 min (*Right*; 55–75 μm) after insertion of a pipette (*) containing ATP (5 mM) and Alexa 594 (50 μM). Note that the position of the pipette was slightly changed during the experiment to ensure that the cell and the pipette were located in the same focal plane. (Scale bar, 5 μm.) (*B*) Representative traces from single trials of Ca^{2+} transients evoked by pressure application of ATP (5 mM, 34 kPa, 100 ms; $n = 6$ cells), the $P2X_7$ agonist Bz-ATP (5 mM, 21 kPa, 100 ms; $n = 4$ cells) and the $P2Y_6$ agonist UDP (100 μM, 34 kPa, 100 ms; $n = 8$ cells).

electroporation as described previously for microglia (28). For details, see *SI Materials and Methods*.

KA Injections. Stock solutions of KA (Sigma-Aldrich) were prepared in 0.1 M PBS at 2 mg/mL. Monocyte-repopulated male B6.FVB-TK+ mice were injected intraperitoneally with 2.5 mg/kg KA and carefully monitored for seizure activity. Mice undergoing status epilepticus for at least 2 h were killed 72 h after KA injection.

Statistical Analysis. Statistical analysis was performed using JMP 7.1 software. The results are expressed as mean values ± SEMs. Student's *t* test was used for comparison of two groups and two-way ANOVA was used for comparison of multiple groups followed by Tukey honestly significant difference (HSD) post hoc analysis.

ACKNOWLEDGMENTS. We thank T. Owens, O. Butovsky, H. Weiner T. Town, K. Rezai-Zadeh, J. Neher, J. K. Hefendehl, C. Schaefer, Y. Eisele, C. Krueger, R. Barbizan Suehs, S. Huber, A. Schlaich, M. Zaichuck, and J. Odenthal for experimental advice and support. Valganciclovir was provided by Roche Bioscience and Roche. This work was supported by the Alzheimer's Association (N.H.V.), The Alexander von Humboldt Foundation (N.H.V.), and German Competence Network on Degenerative Dementias Grant BMBF-01GI0705 (to M.J.).

1. Alliot F, Godin I, Pessac B (1999) Microglia derive from progenitors, originating from the yolk sac, and which proliferate in the brain. *Brain Res Dev* 117:145–152.
2. Ginhoux F, et al. (2010) Fate mapping analysis reveals that adult microglia derive from primitive macrophages. *Science* 330(6005):841–845.
3. Tremblay ME, Lowery RL, Majewska AK (2010) Microglial interactions with synapses are modulated by visual experience. *PLoS Biol* 8(11):e1000527.
4. Wake H, Moorhouse AJ, Jinno S, Kohsaka S, Nabekura J (2009) Resting microglia directly monitor the functional state of synapses in vivo and determine the fate of ischemic terminals. *J Neurosci* 29(13):3974–3980.
5. Nimmerjahn A, Kirchhoff F, Helmchen F (2005) Resting microglial cells are highly dynamic surveillants of brain parenchyma in vivo. *Science* 308(5726):1314–1318.
6. Davalos D, et al. (2005) ATP mediates rapid microglial response to local brain injury in vivo. *Nat Neurosci* 8(6):752–758.
7. Paolicelli RC, et al. (2011) Synaptic pruning by microglia is necessary for normal brain development. *Science* 333(6048):1456–1458.
8. Ransohoff RM, Cardona AE (2010) The myeloid cells of the central nervous system parenchyma. *Nature* 468(7321):253–262.
9. Glass CK, Saijo K, Winner B, Marchetto MC, Gage FH (2010) Mechanisms underlying inflammation in neurodegeneration. *Cell* 140(6):918–934.
10. Perry VH, Gordon S (1991) Macrophages and the nervous system. *Int Rev Cytol* 125: 203–244.
11. Wyss-Coray T (2006) Inflammation in Alzheimer disease: Driving force, bystander or beneficial response? *Nat Med* 12(9):1005–1015.
12. Ajami B, Bennett JL, Krieger C, McNagny KM, Rossi FM (2011) Infiltrating monocytes trigger EAE progression, but do not contribute to the resident microglia pool. *Nat Neurosci* 14(9):1142–1149.
13. Ajami B, Bennett JL, Krieger C, Tetzlaff W, Rossi FM (2007) Local self-renewal can sustain CNS microglia maintenance and function throughout adult life. *Nat Neurosci* 10(12):1538–1543.
14. Mildner A, et al. (2007) Microglia in the adult brain arise from Ly-6ChiCCR2+ monocytes only under defined host conditions. *Nat Neurosci* 10(12):1544–1553.
15. Hawkes CA, McLaurin J (2009) Selective targeting of perivascular macrophages for clearance of beta-amyloid in cerebral amyloid angiopathy. *Proc Natl Acad Sci USA* 106 (4):1261–1266.
16. El Khoury J, et al. (2007) Ccr2 deficiency impairs microglial accumulation and accelerates progression of Alzheimer-like disease. *Nat Med* 13(4):432–438.
17. Naert G, Rivest S (2011) CC chemokine receptor 2 deficiency aggravates cognitive impairments and amyloid pathology in a transgenic mouse model of Alzheimer's disease. *J Neurosci* 31(16):6208–6220.
18. Huitinga I, van Rooijen N, de Groot CJ, Uitdehaag BM, Dijkstra CD (1990) Suppression of experimental allergic encephalomyelitis in Lewis rats after elimination of macrophages. *J Exp Med* 172(4):1025–1033.
19. Fife BT, Huffnagle GB, Kuziel WA, Karpus WJ (2000) CC chemokine receptor 2 is critical for induction of experimental autoimmune encephalomyelitis. *J Exp Med* 192 (6):899–905.
20. Izikson L, Klein RS, Charo IF, Weiner HL, Luster AD (2000) Resistance to experimental autoimmune encephalomyelitis in mice lacking the CC chemokine receptor (CCR)2. *J Exp Med* 192(7):1075–1080.
21. Eichler FS, et al. (2008) Is microglial apoptosis an early pathogenic change in cerebral X-linked adrenoleukodystrophy? *Ann Neurol* 63(6):729–742.
22. Derecki NC, et al. (2012) Wild-type microglia arrest pathology in a mouse model of Rett syndrome. *Nature* 484(7392):105–109.
23. Streit WJ, Xue QS (2009) Life and death of microglia. *J Neuroimmune Pharmacol* 4(4): 371–379.
24. Beers DR, et al. (2006) Wild-type microglia extend survival in PU.1 knockout mice with familial amyotrophic lateral sclerosis. *Proc Natl Acad Sci USA* 103(43):16021–16026.
25. Boillée S, et al. (2006) Onset and progression in inherited ALS determined by motor neurons and microglia. *Science* 312(5778):1389–1392.
26. Grathwohl SA, et al. (2009) Formation and maintenance of Alzheimer's disease beta-amyloid plaques in the absence of microglia. *Nat Neurosci* 12(11):1361–1363.
27. Saederup N, et al. (2010) Selective chemokine receptor usage by central nervous system myeloid cells in CCR2-red fluorescent protein knock-in mice. *PLoS One* 5(10): e13693.
28. Eichhoff G, Brawek B, Garaschuk O (2011) Microglial calcium signal acts as a rapid sensor of single neuron damage in vivo. *Biochim Biophys Acta* 1813(5):1014–1024.
29. Schauwecker PE, Steward O (1997) Genetic determinants of susceptibility to excitotoxic cell death: Implications for gene targeting approaches. *Proc Natl Acad Sci USA* 94(8):4103–4108.
30. Sperk G, et al. (1983) Kainic acid induced seizures: Neurochemical and histopathological changes. *Neuroscience* 10(4):1301–1315.
31. Tondravi MM, et al. (1997) Osteopetrosis in mice lacking haematopoietic transcription factor PU.1. *Nature* 386(6620):81–84.
32. Heppner FL, et al. (2005) Experimental autoimmune encephalomyelitis repressed by microglial paralysis. *Nat Med* 11(2):146–152.
33. Chouery E, et al. (2008) Mutations in TREM2 lead to pure early-onset dementia without bone cysts. *Hum Mutat* 29(9):E194–E204.
34. Neumann H, Takahashi K (2007) Essential role of the microglial triggering receptor expressed on myeloid cells-2 (TREM2) for central nervous tissue immune homeostasis. *J Neuroimmunol* 184(1-2):92–99.
35. Armulik A, et al. (2010) Pericytes regulate the blood-brain barrier. *Nature* 468(7323): 557–561.
36. Bell RD, et al. (2010) Pericytes control key neurovascular functions and neuronal phenotype in the adult brain and during brain aging. *Neuron* 68(3):409–427.
37. Galea I, et al. (2005) Mannose receptor expression specifically reveals perivascular macrophages in normal, injured, and diseased mouse brain. *Glia* 49(3):375–384.
38. Town T, et al. (2008) Blocking TGF-beta-Smad2/3 innate immune signaling mitigates Alzheimer-like pathology. *Nat Med* 14(6):681–687.
39. Butovsky O, Kunis G, Koronyo-Hamaoui M, Schwartz M (2007) Selective ablation of bone marrow-derived dendritic cells increases amyloid plaques in a mouse Alzheimer's disease model. *Eur J Neurosci* 26(2):413–416.
40. Simard AR, Rivest S (2004) Bone marrow stem cells have the ability to populate the entire central nervous system into fully differentiated parenchymal microglia. *FASEB J* 18(9):998–1000.
41. Andersson PB, Perry VH, Gordon S (1991) The CNS acute inflammatory response to excitotoxic neuronal cell death. *Immunol Lett* 30(2):177–181.
42. Zattoni M, et al. (2011) Brain infiltration of leukocytes contributes to the pathophysiology of temporal lobe epilepsy. *J Neurosci* 31(11):4037–4050.
43. Shechter R, et al. (2009) Infiltrating blood-derived macrophages are vital cells playing an anti-inflammatory role in recovery from spinal cord injury in mice. *PLoS Med* 6(7): e1000113.
44. London A, et al. (2011) Neuroprotection and progenitor cell renewal in the injured adult murine retina requires healing monocyte-derived macrophages. *J Exp Med* 208 (1):23–39.
45. Simard AR, Soulet D, Gowing G, Julien JP, Rivest S (2006) Bone marrow-derived microglia play a critical role in restricting senile plaque formation in Alzheimer's disease. *Neuron* 49(4):489–502.
46. Lebson L, et al. (2010) Trafficking CD11b-positive blood cells deliver therapeutic genes to the brain of amyloid-depositing transgenic mice. *J Neurosci* 30(29):9651–9658.
47. Cartier N, et al. (2009) Hematopoietic stem cell gene therapy with a lentiviral vector in X-linked adrenoleukodystrophy. *Science* 326(5954):818–823.
48. Stosiek C, Garaschuk O, Holthoff K, Konnerth A (2003) In vivo two-photon calcium imaging of neuronal networks. *Proc Natl Acad Sci USA* 100(12):7319–7324.
49. Garaschuk O, Milos RI, Konnerth A (2006) Targeted bulk-loading of fluorescent indicators for two-photon brain imaging in vivo. *Nat Protoc* 1(1):380–386.